Chemical Geology 641 (2023) 121781

Contents lists available at ScienceDirect

Chemical Geology

journal homepage: www.elsevier.com/locate/chemgeo

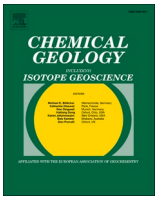

The REY geochemistry of phosphorites during metamorphism of the Haizhou Group, NW Yangtze Block, China

Xiqiang Liu [a,b], Haifeng Fan [a,b,*], Hongjie Zhang [a,b], Chaoyi Xiao [b,c], Haiying Yang [d], Ting Zhou [a,b], Yong Tang [b,c], Pengqiang Shang [e], Chuanwei Zhu [a,b], Hanjie Wen [b,f]

[a] State Key Laboratory of Ore Deposit Geochemistry, Institute of Geochemistry, Chinese Academy of Sciences, Guiyang 550081, China
[b] University of Chinese Academy of Sciences, Beijing 100049, China
[c] Key Laboratory of High-Temperature and High-Pressure Study of The Earth's Interior, Institute of Geochemistry, Chinese Academy of Sciences, Guiyang 550081, China
[d] School of Earth Sciences, Yunnan University, Kunming 650500, China
[e] China Chemical Geology and Mine Bureau, Beijing 100101, China
[f] School of Earth Sciences and Resources, Chang'an University, Xi'an 710054, China

ARTICLE INFO

Editor: Hailiang Dong

Keywords:
Metamorphism
Phosphorite
Phosphate O isotope
Zn isotope
REY remobilization

ABSTRACT

Rare earth elements (REE including Y—REY) in phosphorites have been used widely as a proxy for seawater chemistry at the time of their formation. However, it is unclear whether metamorphism can lead to REE remobilization and alteration of primary seawater signatures recorded in phosphorites. In this study, we examine similarly aged metamorphosed phosphorite ore deposits from the northeastern margin of the Yangtze Block (Jinping and Xinpu ore sections), with contemporaneously deposited unmetamorphosed equivalents in the southwestern margin of the Yangtze Block (Weng'an ore section). New insights have been provided into the migration of rare earth elements and the redistribution of Zn and O isotopes in metamorphosed phosphorite, which suggests that the varying degrees of metamorphic fluid–rock reaction during the metamorphism process significantly reduced the $\delta^{18}O$ value of phosphate (13.7‰ ± 2.2‰ of Jinping phosphate and 7.3‰ ± 1.8‰ of Xinpu phosphate) and added light Zn isotope. These metamorphic fluids were likely generated by the metamorphic dehydration of upper slab uplift during the plate subduction in the Triassic. The negative correlation between the O (and Zn) isotope compositions and REY contents in P-rich rocks suggests that REY were likely re-enriched during the recrystallization process of apatite. Preferential migration of LREE led to significant LREE and MREE enrichment in Haizhou metamorphosed P-rich rocks compared to Weng'an unmetamorphosed phosphorites.

1. Introduction

Ancient and modern phosphorites are rich in associated rare earth elements (REE, including Yttrium), which play critical roles in developing renewable energy supplies (Emsbo et al., 2015; Valetich et al., 2022). Previous studies have largely focused on REE endowment in sedimentary type phosphorite ore deposits (Cook and Shergold, 1984; Emsbo et al., 2015; Yang et al., 2021), with little research conducted on the effect of metamorphism on REY mobilization in phosphorites and the resulting implications on their economic viability. When normalized to the post-Archean Australian Shales (PAAS) (Taylor and McLennan, 1985), there are two main REY patterns in sedimentary apatite: (1) seawater-like patterns, which are characterized by HREE enrichment types and negative Ce anomalies (Emsbo et al., 2015; Shields and Stille, 2001; Valetich et al., 2022); (2) "Bell-shaped" like patterns, which are characterized by pronounced MREE enrichment and depletion of LREE and HREE (Reynard et al., 1999; Zhang et al., 2022). Previous research proposed that the enrichment of REY in phosphorites is mainly controlled by ancient seawater composition (Emsbo et al., 2015; Kim and Kim, 2014), redox-controlled processes during early diagenesis and burial (Elderfield and Sholkovitz, 1987; Valetich et al., 2022), and that the REY compositions are not easily altered during later diagenesis and post-depositional processes such as weathering and transportation (Joosu et al., 2015; Martin and Scher, 2004). Therefore, the REY in phosphorite is often used as a good proxy for tracing initial seawater composition and reconstructing the environment of the paleo-ocean.

* Corresponding author at: Institute of Geochemistry, Chinese Academy of Sciences, 99 Lincheng West Road, Guanshanhu District, Guiyang 550081, China.
E-mail address: fanhaifeng@mail.gyig.ac.cn (H. Fan).

https://doi.org/10.1016/j.chemgeo.2023.121781
Received 6 June 2023; Received in revised form 11 October 2023; Accepted 12 October 2023
Available online 16 October 2023

However, it is unknown if the REY in phosphorite retain the original composition after undergoing the metamorphism.

In South China, abundant phosphate rock resources were distributed along the Yangtze block (YZB) during the Ediacaran (ca. 635 Ma - 551 Ma) (Cook and Shergold, 1984; Graham and Lawrence, 2011). Among them, phosphorites distributed along the northeast margin of the YZB underwent metamorphism during the Triassic, while their equivalents in the central and southwest margins of the YZB did not. Metamorphosed phosphorites are mainly distributed in Haizhou County of northern Jiangsu Province, Feidong County in central Anhui Province, Susong County in southwestern Anhui Province, and Dawu in eastern Hubei Province (Sang, 1991; Yao and Xiong, 1994). The Jinping and Xinpu phosphorite ore sections in Haizhou Country, now as a part of the high-pressure, low-temperature Sulu Orogenic Belt (SOB), host the exposed sections of the metamorphosed phosphorites (Fig. 1) (Prave et al., 2018; Xiong and Yao, 1996). Doushantuo Formation in the central and western YZB is an unmetamorphosed equivalent to the metamorphosed phosphorites in the Haizhou County (Jinping and Xinpu ore sections). Numerous geochemical and isotopic studies have been performed on the phosphorites in the Doushantuo Formation (Weng'an phosphorites are typical representative) (Cui et al., 2015; Ling et al., 2007; Ohno et al., 2008), thus allowing for direct comparison of metamorphosed and

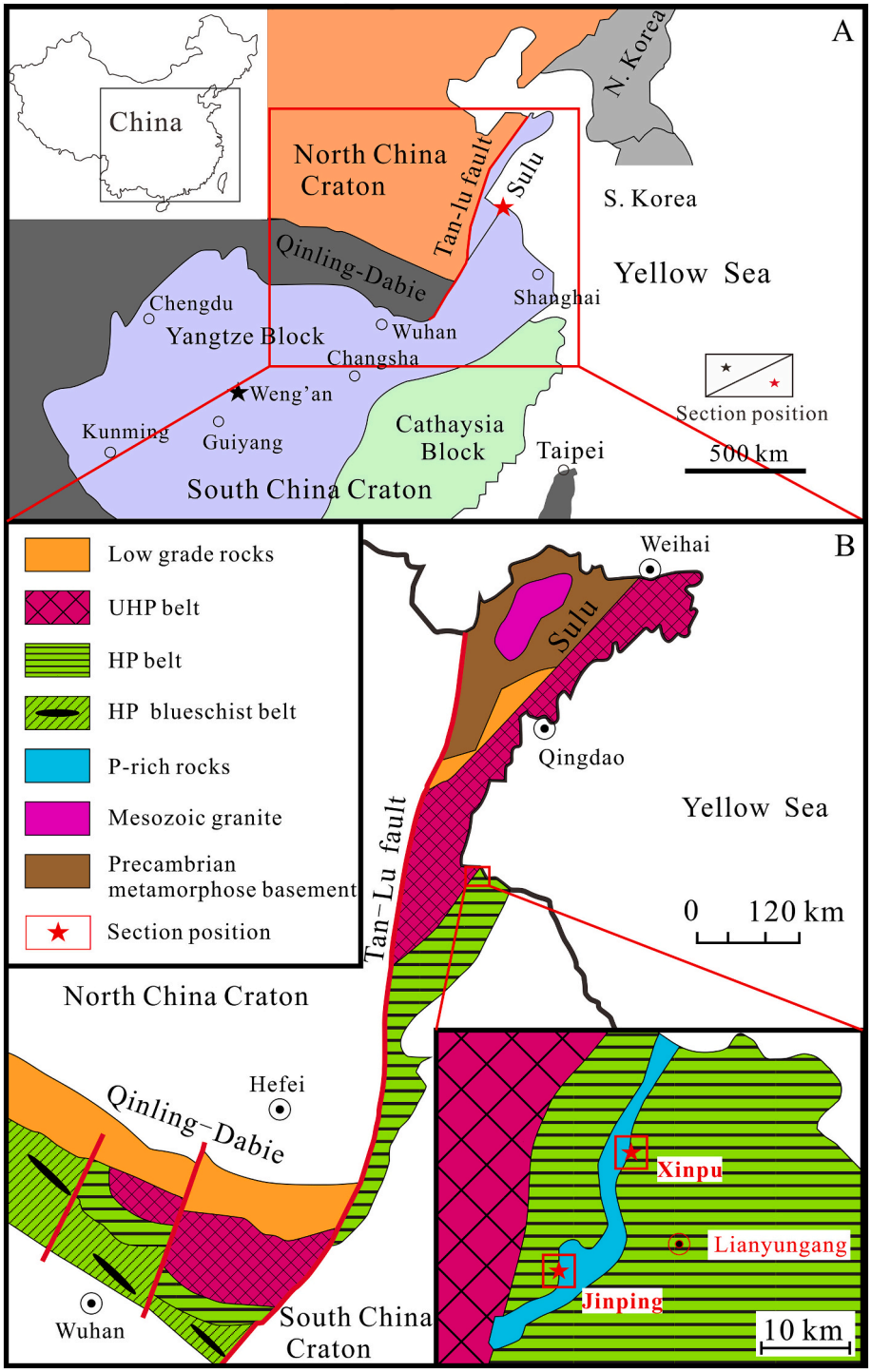

Fig. 1. Ore section location (A), tectonic sketch map of Sulu belt and distribution of phosphorites (B), after Zheng et al. (2008a) and Prave et al. (2018).

unmetamorphosed phosphorite sections and the ensuing remobilization and enrichment/depletion of REY during the metamorphic process.

Oxygen isotope compositions vary between different rock types depending on their origin. Generally, terrigenous sediments yield high $\delta^{18}O$ values (~15–25‰), igneous rocks typically yield lower $\delta^{18}O$ values (~6–10‰), while metamorphic rocks have highly variable $\delta^{18}O$ values due to nature and origin of the metamorphic fluids they have interacted with (Valley, 2019). A single study on the oxygen isotope composition of phosphate showed Ediacaran phosphorites has high $\delta^{18}O$ values (15–17.9‰) (Yang et al., 2021). These values provide a starting oxygen isotopic composition for the evaluation of the effect of metamorphism and metamorphic fluids on REY mobilization in phosphorites.

The zinc isotopic composition ($\delta^{66}Zn$) of geological reservoirs can reflect the mechanism of different geological processes and geological events, as well as the geochemical cycle of zinc in nature (Little et al., 2014; Liu et al., 2022; Wang et al., 2017b; Yan et al., 2019). Generally, mantle materials ($\delta^{66}Zn$ = ~0.20‰) (Wang et al., 2017b), terrestrial sediments ($\delta^{66}Zn$ = ~0.27‰) (Little et al., 2014), and rivers ($\delta^{66}Zn$ = ~0.33‰) have lighter Zn isotope compositions (Sossi et al., 2018), but marine phosphorites in the Weng'an section are typically enriched in heavier Zn isotopes (~0.8) (Fan et al., 2018b). However, involvement of metamorphic fluids may shift the Zn isotopic compositions to change towards a lighter or heavier isotopic signatures depending on the characteristics of the metamorphic fluids. Hence, a combination of oxygen and Zn isotopic compositions in phosphorite can provide information on the degree of interaction of primary phosphorites and exogeneous metamorphic fluids.

This study aims to determine the impact of metamorphism on mobility of REY in sedimentary phosphorites by integrating whole rock Zn and phosphate O isotopic compositions, along with major and trace element geochemistry of metamorphosed (Haizhou sections) and unmetamorphosed (Weng'an sections) phosphorites in the Yangtze Block, south China.,.

2. Geological setting

The South China Craton, as a part of the Rodinia supercontinent, was formed by the amalgamation of the Yangtze and Cathasia Blocks (Fig. 1. A) during the Tonian Jiangnan orogeny (Cawood et al., 2018; Wang et al., 2014; Zhao and Cawood, 2012). During the late Neoproterozoic,

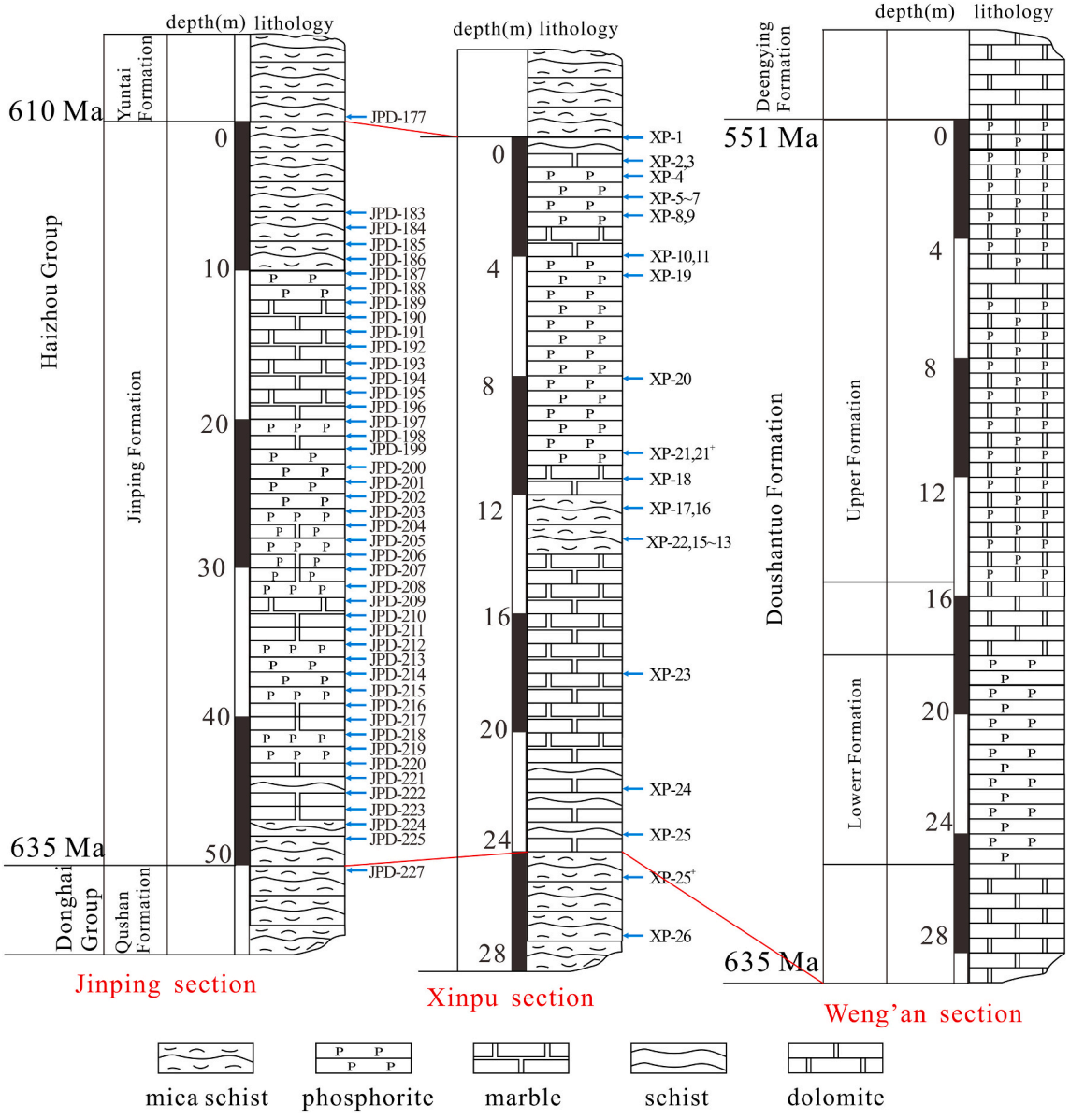

Fig. 2. Profile of Jinping, Xinpu, and Weng'an ore section (Yang et al., 2021).

the Yangtze block developed into an extensive shallow-marine carbonate platform-slope-basin, accompanied by a large number of phosphorite deposits, such as the Weng'an phosphorite deposit in central Guizhou and Yichang phosphorite deposit in Hubei (Algabri et al., 2020; Cui et al., 2016; Prave et al., 2018; Tahata et al., 2013; Wang et al., 2014). The northern margin of the Yangtze Block experienced subduction under the North China Block and subsequent high-P, low-T metamorphism during the continental collision in the Triassic that resulted in metamorphism of the Neoproterozoic marine sedimentary rocks, including carbonates and phosphorites that form part of the Haizhou Group sediments. Recent studies have shown that the strata of the Jinping Formation of the Haizhou Groupe are likely equivalent to the Doushantuo Formation (635–551 Ma, Fig. 2) based on the results of the carbon isotope analysis of carbonate, U—Pb isotope, and Lu—Hf isotope of zircon (Li et al., 2011; Ling et al., 2007; Liu et al., 2004; Sato et al., 2016; Zhou et al., 2012).

Previous studies reported that UHP metamorphic rocks, such as eclogites in the Sulu orogenic belt, recorded the subduction of the YZB under the North China block (NCB), and subsequent exhumation at 250–202 Ma (Xu et al., 2003). In the exhumation process, some eclogites underwent retrograde metamorphism to varying degrees (Zong et al., 2010), which resulted in, the fluid remobilization of elements that have affected the rocks within the collision zone (Xu et al., 2003).

The Haizhou Group can be divided into two formations (the Jinping and Yuntai Formations). The underlying bedrock is the Qushan Formation of the Donghai Group (Fig. 2). The metamorphic rocks in the Jinping and Xinpu ore sections are mica schist, gneiss, marble, and metamorphosed phosphorite. Previous studies suggested that metamorphic rocks in this area underwent blueschist to greenschist facies in regional metamorphism, which contrasts the primary overall subduction zone HP metamorphism at 350–450 °C and 0.6–0.85 GPa, equivalent to subduction to a depth of 30 km (Prave et al., 2018; Wang et al., 2017a; Zhou et al., 2012).

3. Materials and methodologies

In this study, two type sections currently in production (Xinpu and Jinping) were selected for sample collection in the fieldwork. The Jinping and Xinpu phosphorite ore deposits of the Haizhou Group, including 27 samples in the Xinpu deposit and 45 samples in the Jinping Deposit, were investigated. The samples were fresh and sequential, including the overlying strata, ore-bearing formation, and the underlying strata. The specific rock types and serial numbers are listed in Table S1. All samples were made into thin sections and observed under the polarizing microscope. Seventy-two samples were analyzed to determine their major and trace element compositions (Table S1). Thirteen samples were analyzed to determine the in-situ trace element compositions (Table S2-S4). Sixteen samples and twenty-three samples were selected to determine the phosphorate oxygen and whole-rock zinc isotopes, respectively (Table S5). Detailed analytical methods are described below.

3.1. Major and trace element analyses of whole rocks

The major elemental components of phosphorites and host rocks were analyzed at the Institute of Geochemistry, Chinese Academy of Sciences (IGCAS) by X-ray fluorescence (XRF, ME-XRF06). Phosphorite samples were digested using a $LiNO_3$ solution, and the host rocks were digested with $Li_2B_4O_7$ and then melted at 1000 °C for 2 h. The sum of XRF analyses and loss on ignitions (LOIs) was considered the "sum total" with a standard deviation of <1%. The detection limits of trace elements are as follows: Ce, Ho, Lu, Tb, and Tm (~0.01 ppm); Er, Eu, Pr, Sm, and Yb (~0.03 ppm); Dy and Gd (~0.05 ppm); Yand Nd (~0.1 ppm); Sr and Th (~0.2 ppm); La and Zr (~0.5 ppm). The relative error and relative deviation were < 10%. Trace element analyses were conducted at IGCAS using a quadrupole inductively coupled plasma mass spectrometer (QICP-MS), model ELAN-DRC-e ICP-MS, with a relative standard deviation generally better than 10%. Portions (50 mg) of the samples were digested completely using a mixed HF and HNO_3 solution for 72 h. The analytical method was performed using the methodology reported by (Liang et al., 2000). The detection limits were as follows: Tb, Ho, Lu, and Tm (0.01 ppm); Er, Eu, Sm, Pr, and Yb (0.03 ppm); Ce, Gd, and Dy (0.05 ppm); Hf (0.2 ppm); Nd (0.1 ppm); Y and La (0.5 ppm); and Zr and Mo (2 ppm).

3.2. In situ trace element analyses

The in-situ trace elements of apatite were analyzed at IGCAS using the GeoLasPro laser ablation system (193 nm, premixed gas, IIIb safety level, 95% confidence level). Operating conditions included a 44-μm spot size at 5 J/cm^2 and 10 Hz with an 18 s baseline and 50 s ablation. Using NIST610, NIST612, NIST614, and Durango apatite as the standard samples, the apatite trace element compositions were quantified using a standard sample bracketing method. The internal corrections were applied using the element abundances of Ca determined by EMPA analyses to correct matrix effects between the standards and the analyzed minerals (Liu et al., 2008). The signal was processed with LA-ICP–MS Data Reduction Software (ICPMCDataCal) developed by Liu et al. (2008) using sample bracketing method (Chew et al., 2016). The reference element contents of the external standards are available online at https://georem.mpch-mainz.gwdg.de/.

3.3. Phosphate O isotopes

In this study, the phosphate separation and purification method established by Blake et al. (2010) was used to measure the oxygen isotope composition of phosphate in the sample. This method is effective for the separation and purification of phosphate in a complex matrix. Samples were extracted with 50 mL of 1 M HCl. The ratio of sample mass to solution volume was 1 g: 50 mL. Shaking extraction was performed on a shaking table for 16 h. The supernatant was collected after centrifugation. Phosphate was further separated and purified by the ammonium phosphomolybdate-magnesium ammonium phosphate (APM-MAP) precipitation method. The MAP solute passes through a cation exchange resin (H^+ type) and anion exchange resin column (HCO_3^- type) to remove cations (such as Mg^{2+}) and residual dissolved organic matter (Colman, 2002). The $NaHCO_3$ eluate was sonicated under acidic conditions (pH < 1), and N_2 was introduced to remove HCO_3^-. Finally, PO_4^{3-} was converted into Ag_3PO_4 precipitation by the ammonia volatilization method (Firsching, 1961). The Ag_3PO_4 precipitate was centrifugally washed with ethanol and Milli-Q water several times. After no Ag^+ residue was detected in the washing solution, the precipitate was dried at 60 °C and stored in the dark. The formed Ag_3PO_4 was measured by a pyrolysis-isotope ratio mass spectrometer to measure $\delta^{18}O_P$. The (Vienna) Standard Mean Ocean Water (SMOW) was used as the $\delta^{18}O$ standards (Coplen et al., 1983) and the isotope ratio mass spectrometer with a precision (2σ) of 0.1‰.

3.4. Zn isotopes of phosphorite

The Zn isotopes of phosphorite were analyzed at the IGCAS. The method established by Tang et al. (2006) is mainly used for chemical purification and instrument testing of Zn isotopes. The powder geological sample was weighed quantitatively (depending on the content of Zn in the sample) and digested in aqua regia at 120 °C. The dissolved sample was converted to 7 N HCl + 0.001% H_2O_2 medium. Using an AG-MP-1 ion exchange column, Zn was eluted with 10 mL of 2 N HCl + 0.001% H_2O_2 medium to separate Zn from other interfering elements. The eluent was collected, and then the medium was converted to a 1% HNO_3 medium after dryness. MC-ICP–MS is used to measure zinc isotopes. In the test process, the standard sample crossover method was used to correct the instrument quality discrimination effect, and GSB Zn

was used as the zinc isotope standard. A standard-sample bracketing approach was applied to correct the instrumental mass discrimination when an IRMM3702 Zn solution was used as the working standard (Fan et al., 2018a), where $\delta^{66}Zn = [(^{66}Zn/^{64}Zn)\ sample/(^{66}Zn/^{64}Zn)_{\ Lyon\ JMC} - 1] \times 10^3$. All $\delta^{66}Zn$ values are reported compared to the JMC Lyon Zn standard based on the published difference between IRMM3702 Zn and JMC Lyon Zn ($\Delta^{66}Zn_{\ IRMM3702\text{-}JMC\ Lyon\ Zn} = +\ 0.30‰$, (Vance et al., 2016)). The $\delta^{66}Zn$ values of BHVO-2 (0.30 ± 0.03‰), COQ-1 (0.28 ± 0.06‰), and NIST 683 (0.16 ± 0.05‰) are consistent with previous publications (Fan et al. (2018b) and Liu et al. (2023) and reference therein).

4. Results

4.1. Petrological characteristics

Samples in the Xinpu and Jinping ore sections mainly contain quartz schist, mica schist, phosphorite (P_2O_5 > 18 wt%), apatite-bearing marble (10 wt% > P_2O_5 > 18 wt%), marble and schist. The P-rich rocks are mainly phosphorite and apatite-bearing marble (in this text, we collectively refer to it as P-rich rocks). The marble and phosphorite were collected in the middle part of both two ore sections. Among them, marble is composed of ~80% dolomite, with minor amount of muscovite, apatite, quartz and pyrite; phosphorite is composed of 50–90% apatite, 5–40% dolomite and calcite, with minor amount of biotite and muscovite, apatite and pyrite (Fig. 3.A, C, E); apatite-bearing marble is composed of 50–80% dolomite, and ~ 10–48% apatite, with minor amount of quartz, biotite and pyrite. Both the hand specimens and microscopic photos of phosphorites show clear calcite veins (bedding parallel, Fig. 3.A, C, E) penetrating through the rock mass, indicating the widespread presence of metamorphic hydrothermal fluids.

The quartz schist was collected in the lower and upper part of the Jinping Formation. It is composed of quartz (55–65%), plagioclase (10–15%), feldspar (15–25%), muscovite (5–10%) with minor amounts of apatite, pyrite, zircon and rutile (Fig. 3.B, D, F). The mica schists were collected in the lower and upper part of the Jinping Formation, which is strongly foliated with completely recrystallized structures, mainly composed of schistose and columnar minerals: quartz (35–50%) plagioclase (15–25%), muscovite (15–20%), biotite (5–10%) calcite (5–10%), with minor amounts of apatite, pyrite. Mica schists that are interbedded with the metamorphosed dolomite and phosphorite rock packages comprise muscovite, quartz, plagioclase and calcite rich mineral assemblages suggesting they likely underwent lower grade (greenschist facies) metamorphism. This is consistent with previous estimations of metamorphic grades which yielded temperature and pressure values of at 350–450 °C and 0.6–0.85 GPa respectively (Prave et al., 2018; Wang et al., 2017a; Zhou et al., 2012). Compared to Weng'an cemented quartz, the edge of quartz in the metamorphosed phosphorites shows a sickle shape, indicating it has undergone recrystallization (Fig. 3.G). Apatite displays redundant colloidal, crystalline granular, idiomorphic, and allomorphic crystals. Apatite has common cracks, and the apatite boundary is replaced by quartz into a harbor shape (Fig. 3.G). Under the scanning electron microscope, apatite is mostly a hexagonal short column, arranged in clusters, and most of the collophanite has been recrystallized into apatite. Cracks are developed on the surface of apatite, and intact collophanite spherical structure can be seen in the cracks (Fig. 3.H).

4.2. Major and trace elements of phosphorite and host rocks

Table S1 lists the whole rock major and trace element contents of the Xinpu and Jinping phosphate ore samples. The ∑REY (sum of lanthanides, including Y) of phosphorites varied from 3.14 to 576.59 ppm. P-rich rocks with high REY contents (>100 ppm) are mostly developed at the bottom and top of both two sections in contact with mica schist. There are two types of REY patterns of phosphorites when normalized to Post Archean Australian Shale (PAAS) (Taylor and McLennan, 1985): 1) MREE enrichment patterns with high REY content (>100 ppm) and high Gd_N/Yb_N ratios (1.5–2.1, mean 1.8, Fig. 4.A), which is similar to Weng'an P-rich rocks (Fig. 4.B); 2) Flat patterns with low REY content (<100 ppm) and marginally lower Gd_N/Yb_N ratios (0.9–1.7, mean 1.2, Fig. 4.C). Some marbles in ore bodies show HREE enrichment patterns with low REY contents and Gd_N/Yb_N ratios (0.2–0.6, mean 0.5, Fig. 4.D), while the other marbles and most of the mica schists show flat REY patterns (Fig. 4.E). The REY patterns of basal and overlying rocks show obvious different patterns compared to the P-rich rocks and marbles from within the ore body (Fig. 4.F).

4.3. In situ trace elements of apatite

The in-situ REY of the Xinpu and Jinping minerals are listed in Tables S3. There are three types REY patterns of apatite when normalized to PAAS: 1) MREE enrichment patterns with high REY content (>100 ppm) and Gd_N/Yb_N ratios (mean 2.2, Fig. 5.A); 2) HREE depletion patterns with low REY content (<50 ppm) and high La_N/Yb_N values (mean 4.75, Fig. 5.B), with one sample displaying medium REY (mean 65 ppm) and La_N/Yb_N values (mean 2.23); 3) flat REY patterns with no obvious anomaly (Fig. 5.C). The carbonate in host rocks shows HREE enrichment patterns and flat REY patterns marginally enriched in HREE (Fig. 5.D). Notably, the REY content of gangue minerals and some apatite is very low (some contents are below the detection limit), thus a rough trend is provided here.

4.4. Phosphate O isotopes and phosphorite Zn isotopes

Table S5 lists the phosphate O isotopic compositions, with SMOW as the standard. The $\delta^{18}O_P$ of seven samples in the Xinpu ore section and nine samples in the Jinping ore section varied from 4.0‰ to 8.9‰ (δ = 1.6576, n = 7) and 10.0‰ to 16.2‰ (δ = 2.054, n = 9), respectively. The $\delta^{66}Zn$ values of 10 samples in the Xinpu ore section and 13 samples in the Jinping ore section were 0.29–0.42‰ (δ = 0.036, n = 10) and 0.49–0.68‰ (δ = 0.054, n = 13), respectively.

5. Discussion

5.1. The age and REY source of Haizhou metamorphosed P-rich rocks

The youngest detrital zircons in quartz–mica schist from the lower part of the Jinping Formation give concordant ages of 635 ± 9 to 654 ± 16 Ma (Zhou et al., 2012), indicating that the rocks are not older than ~635 Ma, equivalent to the bottom boundary of the Doushantuo Formation. Neoproterozoic magmatism is widely distributed across South China and is commonly linked to the breakup of Rodinia (Zheng et al., 2008a). Two major phases of bimodal magmatism occurred during the Neoproterozoic in South China; at 740–780 Ma and 800–830 Ma (Zheng et al., 2008b). Zircons from the siliciclastic Haizhou Group have U—Pb ages showing two prominent peaks at 758 and 828 Ma, indicating that the sources of the Haizhou Group were most likely Neoproterozoic granitoids and possibly contemporaneous volcanic rocks (Zhou et al., 2012).

There are two types of REY patterns recorded by Weng'an phosphorites of the Doushantuo Formation, in which the Lower phosphorites show seawater-like patterns, and the Upper phosphorites show MREE enrichment patterns (Yang et al., 2021). Except for the samples of Upper of Weng'an phosphorites, the Haizhou P-rich rocks and the samples from the lower part of Weng'an did not show a correlation between P and REY (Fig. 6.A), suggesting that besides apatite, there are other minerals carrying REY. In situ data of apatite indicate that high REY content apatite shows good correlations between P and REY in both the Xinpu and Jinping section (Fig. 6.B, C), which indicate that apatite is the main carrier of REY in Haizhou metamorphosed P-rich rocks. However, some metamorphosed phosphorites with low REY contents (<100 ppm, flat or

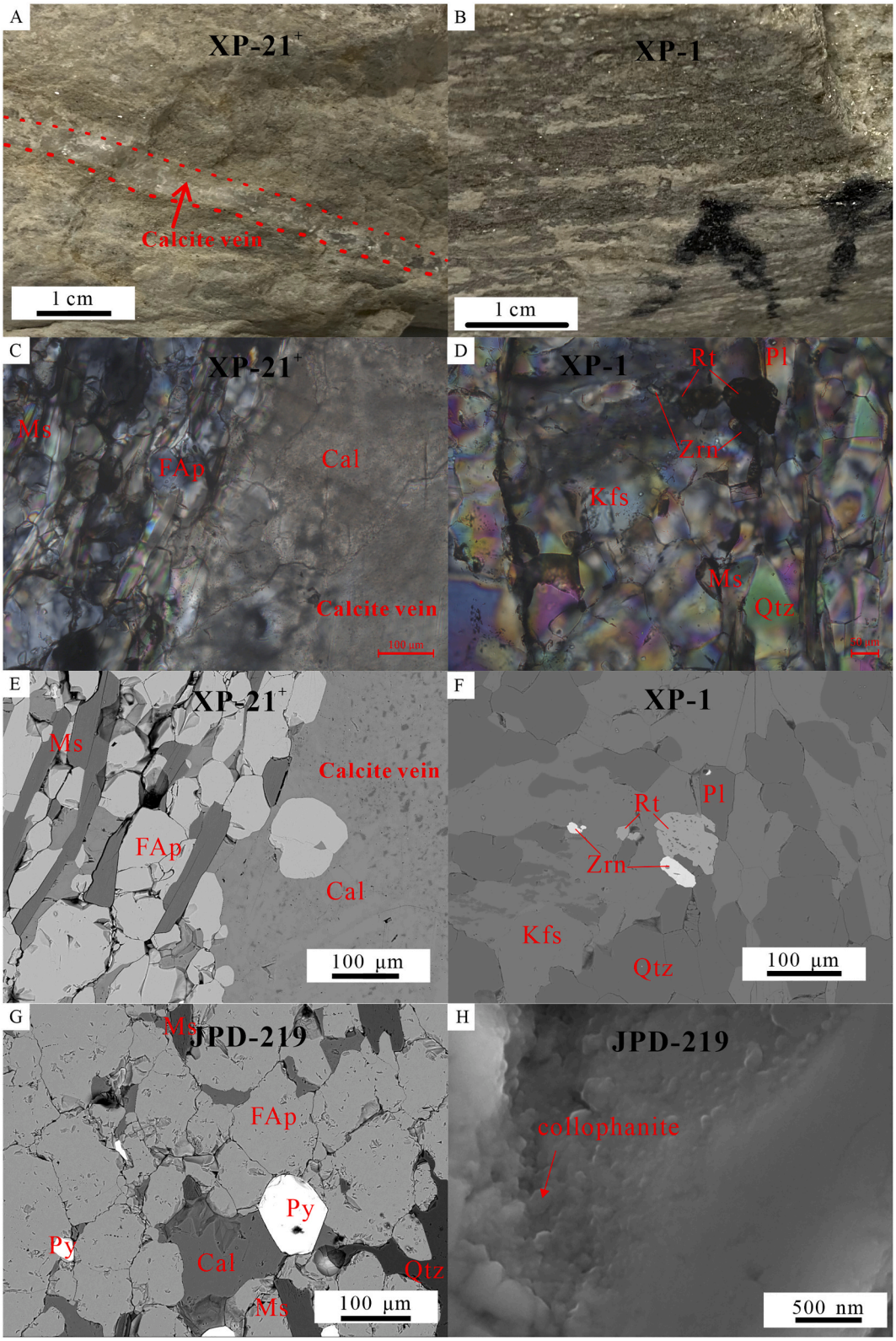

Fig. 3. Textural and petrological characteristics of the samples of the Xinpu and Jinping ore section. Image A, C and E are from phosphorites in the lower part of profile (XP-21^{+}); B, D and F are from quartz schist of upper part of P-rich ore body (XP-1), G and H from phosphorites in the lower part of profile (JPD-219). A and B: hand specimen photos; C and D: orthogonal polarized photos; E, F, G and H: SEM images. Cal = calcite; FAp = fluorapatite; Ms. = muscovite, Py = pyrite, Qtz = quartz, Pl = plagioclase, Kfs = K feldspar, Zrn = Zircon, Rt = Rutile.

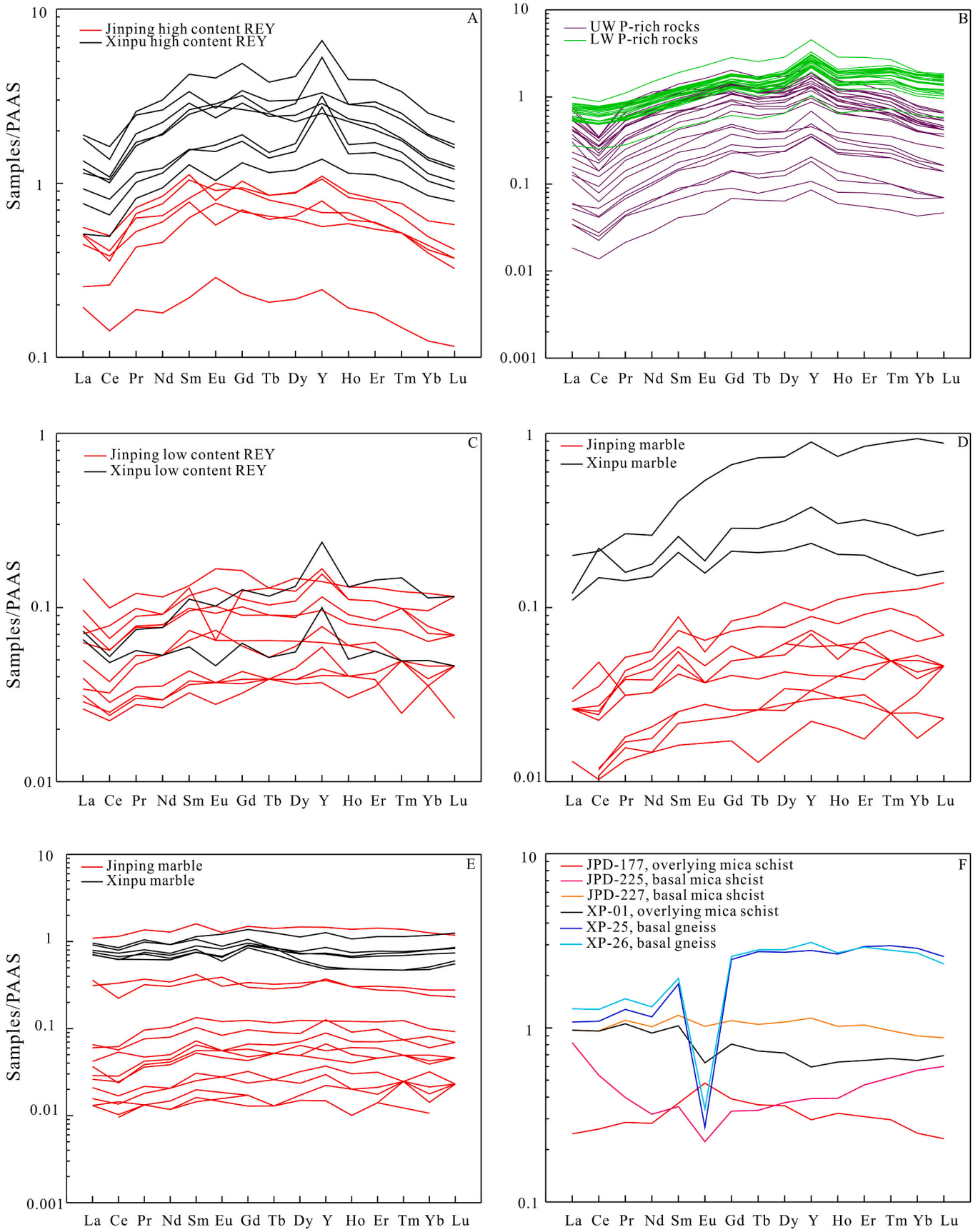

Fig. 4. PAAS-normalized patterns of whole rocks. A and C: REY patterns of Haizhou P-rich rocks; B: REY pattern of Weng'an phosphorites (Yang et al., 2021); D and F: REY patterns of Marbles surrounding the Haizhou P-rich rocks; F: REY patterns of the upper and lower samples of whole profiles.

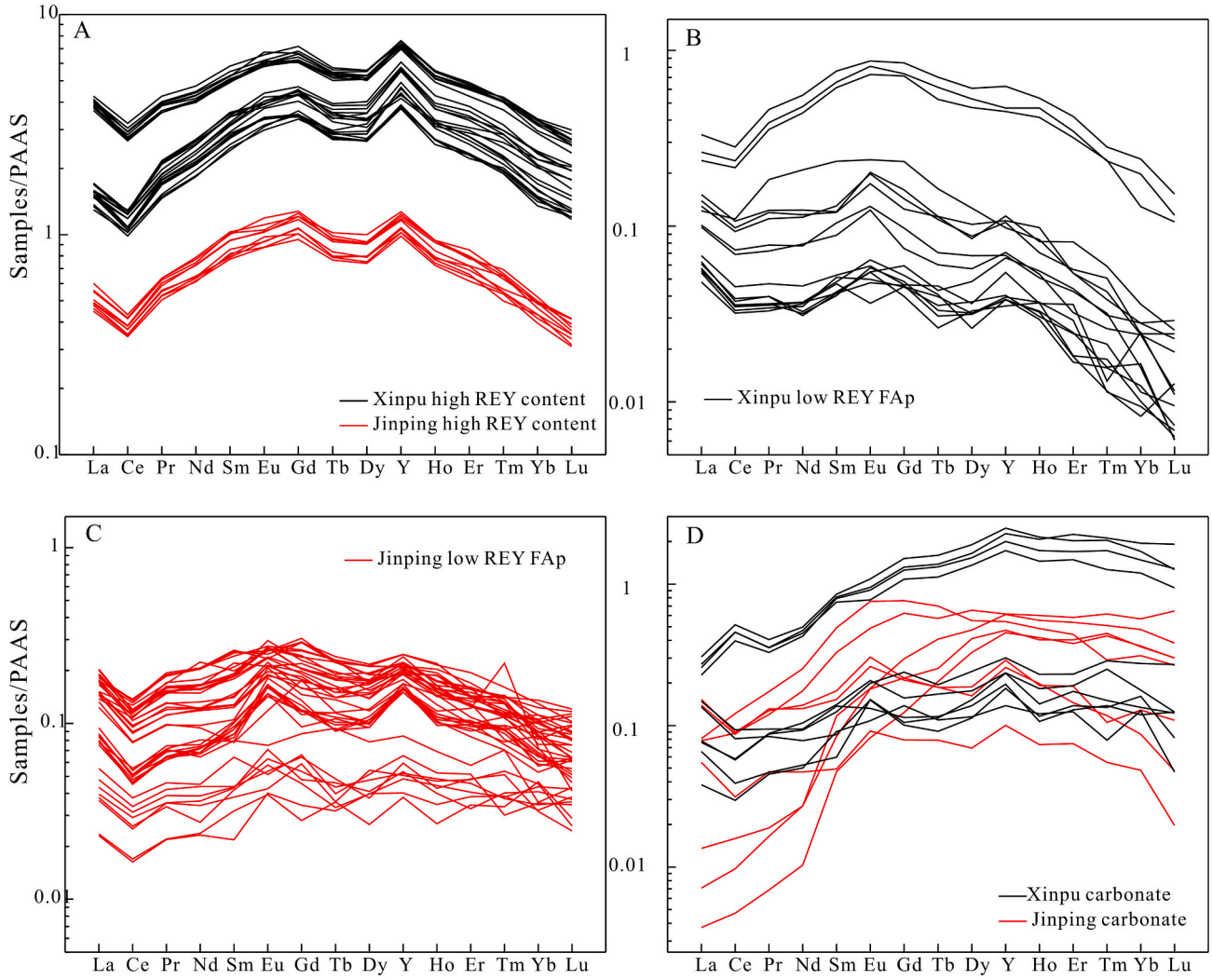

Fig. 5. PAAS-normalized patterns of apatite and ganged minerals. A-C: REY patterns of Haizhou apatite; D: the REY pattern of carbonate surrounding the apatite.

HREE depleted patterns) display the obvious different REY patterns from the Weng'an ore section.

Previous studies inferred that the REY contents in the Doushantuo phosphorites were mainly affected by hydrothermal fluids and paleo-oceanographical environment (Chen et al., 2003; Yang et al., 2021; Yu et al., 2023). Hydrothermal fluids may also be an important source of REY in seawater. Yu et al. (2023) found the positive Eu anomalies (Eu/Eu* >1) recorded by the Doushantuo phosphorites, indicating the contribution of hydrothermal fluids to the REY content of seawater. However, most of the P-rich rocks in Weng'an and Haizhou did not display Eu anomalies (Fig. 6.D), indicating that the REY recorded by our samples are not related to hydrothermal activity.

In the early Ediacaran, the seawater environment was characterized by reduction, which was recorded by high Ce/Ce*(~0.90, Fig. 6.E) in phosphorites (Yang et al., 2021). However, in the late Ediacaran, the seawater became an oxidizing environment, and the Ce/Ce* (~0.58, Fig. 6.E) recorded in phosphate rocks decreased (Yang et al., 2021). It was not until the early Cambrian that Ce/Ce* (~0.32) reached a new low value, and ocean had completely oxidized by this time (Wen et al., 2015; Yang et al., 2021) The Ce/Ce* (~0.76, Fig. 6.E) recorded in our samples are within the range of Ediacaran phosphorites. In addition, unlike the high Y/Ho value of seawater (44–83) (Bau et al., 1997), the Y/Ho values (Fig. 6.F) recorded by Weng'an (~40) and Haizhou P-rich rocks (~37) are significantly lower. Yang et al. (2021) indicated that the lower Y/Ho values may represent the increase of terrestrial inputs. The Ce/Ce * and Y/Ho values recorded by the Haizhou metamorphosed P-rich rocks are similar to those of the Weng'an unmetamorphosed phosphorites. Overall, Haizhou Group metamorphosed phosphorites are lower than the Weng'an unmetamorphosed section (Fig. 6F) further supporting metamorphic recrystallisation of the Haizhou Group phosphorites (and in particular Jinping section).

However, Y/Ho and Ce/Ce* can be altered during later diagenesis or recrystallizition (Shields and Stille, 2001), especially after undergoing metamorphism, while Ce anomalies remain largely unchanged. In addition, Y/Ho and Ce/Ce* cannot explain why the samples show more enrichment in LREE and MREE, nor explain the different types of REY patterns in low REY content samples. Reynard et al. (1999) proposed that the La_N/Sm_N vs. La_N/Yb_N diagram can be used to decipher different mechanisms of REE incorporation into apatite. The La_N/Yb_N ratios are not affected during substitution but show an increase if the adsorption mechanism dominates. Meanwhile, the La_N/Sm_N ratios usually remain invariant during absorption but decrease during substitution (Zhu and Jiang, 2017). The higher La_N/Yb_N and lower La_N/Sm_N ratios in apatite relative to seawater may indicate that early and late diagenesis occurred, respectively. La_N/Sm_N - La_N/Yb_N characteristics (Fig. 7.A, B) recorded by P-rich rocks and apatite show the high REY samples fall into (or close to) the range of seawater, indicating the majority of the REY comes from the apatite, and high REY samples with lower La_N/Sm_N and La_N/Yb_N may be affected by partly recrystallization.

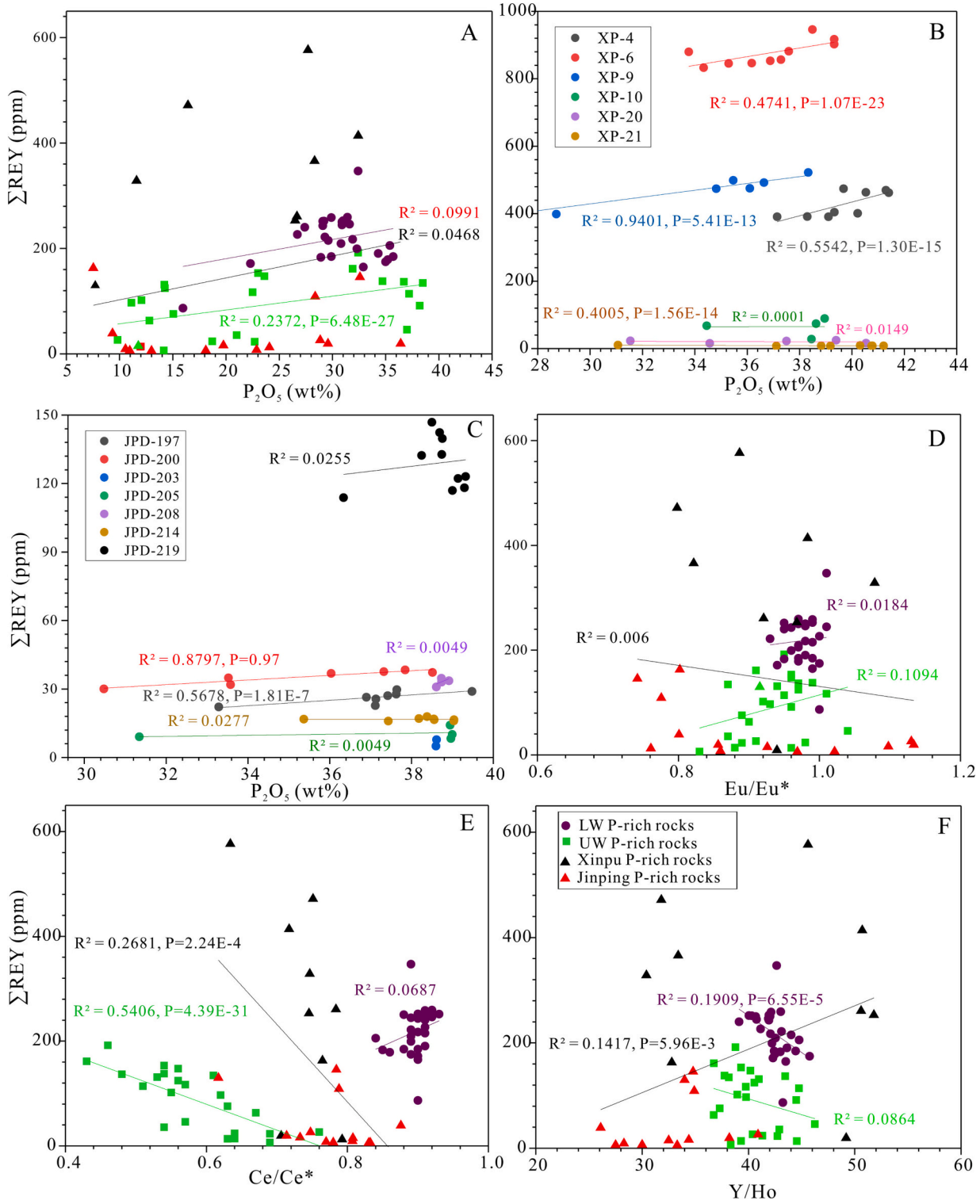

Fig. 6. A: The correlation diagrams of P_2O_5 vs. REY in whole rocks of Haizhou and Weng'an P-rich rocks; B and C:The correlation diagrams of P_2O_5 vs. REY in Haizhou apatite. D-F: Eu/Eu*, Ce/Ce* and Y/Ho vs. REY in whole rocks of Haizhou and Weng'an P-rich rocks (Yang et al., 2021). R^2 is the judgment coefficient, and P is *P*-values.

5.2. *Influence of metamorphism on Haizhou phosphorite*

5.2.1. *The ^{18}O-depleted fluid recorded in metamorphosed phosphorites*

The metamorphic recrystallization of minerals can cause the fractionation of trace elements. This process can proceed via the mineralogical mechanism of solid-state transformation, replacement alteration, and/or dissolution reprecipitation (Xia et al., 2010). Mineral oxygen isotopes may maintain the properties of the original rock in an anhydrous environment, while partial or complete resetting may occur with the participation of metamorphic water (Chen et al., 2011). The O isotopic redistribution between different minerals may occur during the metamorphic process.

In the subducting oceanic plate, metasediments will interact with fluids from both the dehydrating crust and mantle (Zack and John,

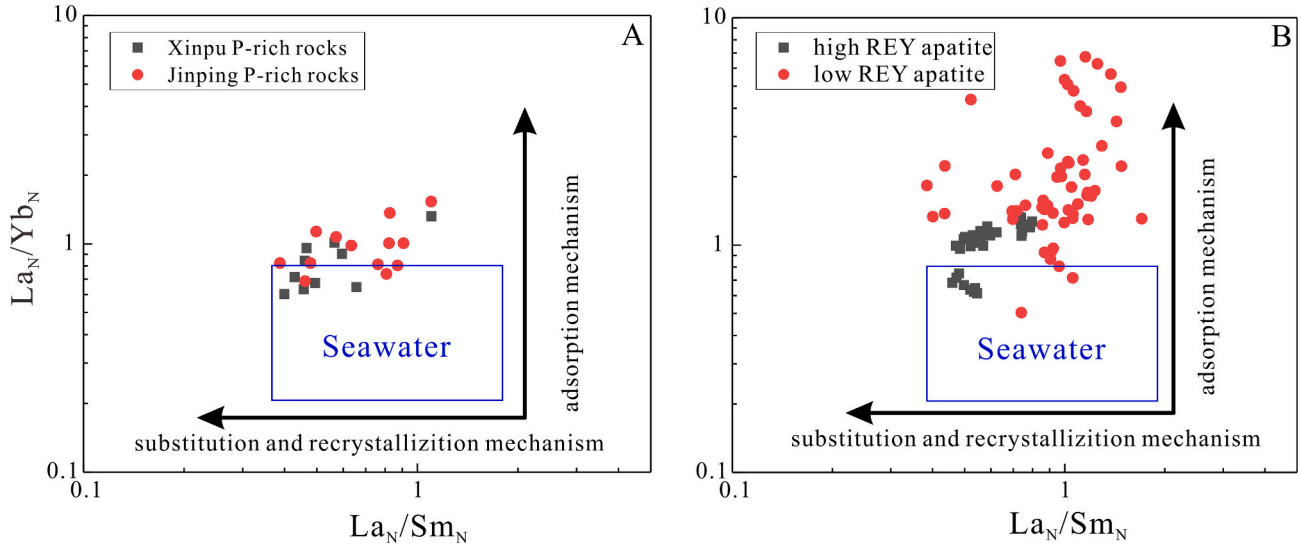

Fig. 7. A: The correlation diagrams of La_N/Sm_N vs. La_N/Yb_N of Haizhou P-rich rocks; B: The correlation diagrams of La_N/Sm_N vs. La_N/Yb_N Haizhou apatite.

2007). The oxygen isotope value of the mantle is limited to ~0.57 (Bindeman, 2008). Permeabilities in the subducting slab appear to be too low and dihedral angles between fluid and relevant minerals too high to allow for porous flow (Manning and Ingebritsen, 1999), hence fluid channelization is critical for the understanding of subduction zone fluid fluxes. Most devolatilization reactions are strongly occur as the temperature rises during ongoing subduction (Schmidt and Poli, 1998), while in the upper of the slab, the sediments release water first, followed by the crust and then the mantle (Hacker et al., 2003). Since a decrease of solid volume, associated with dehydration reactions, increases porosity and hence permeability (Wang and Wong, 2003), if sufficiently high volumes of fluid are reached, the elevated fluid pressure can open fractures, thus allowing long-distance fluid transport (Jung et al., 2004). In addition, selvages and shear zones can provide a place for interaction between long-distance fluids and their enclosing host rocks, facilitating ion exchange and modifying the composition of fluids substantially along flow paths (Breeding et al., 2004). Aqueous fluid produced by dehydration reactions will not percolate through large rock volumes, but rather will be carried away from the dehydration sites by a veining network. In our samples, obvious calcite veins (Fig. 3.A) were found to penetrate the phosphorites and apatite-bearing marbles, which confirm the existence of fluid channelization and the involvement of metamorphic fluids.

Previous studies indicated large lithophile elements (LILE's) generally show the highest mobilities, followed by LREE and then HREE during the plate subduction (Zack and John, 2007). In addition, among the high field strength elements (HFSE), even Th and Nb shows higher mobilities. Therefore, the upward migration of metamorphosed fluids will significantly enrich in LILE's such as K, Rb and B. Interestingly, the O isotopic compositions of phosphorites and apatite-bearing marbles showed varying degrees of negative correlation with K Rb, Ba Nb and Th (Fig. 8A-E), which indicate that the samples with lighter oxygen isotopic compositions (compared to the Weng'an phosphorites) were likely caused by the additions of lower $\delta^{18}O$ water-bearing metamorphic fluids. Negative correlation between the O isotope values and the insoluble HFSE elements (Th and Nb), in particular, indicates the widespread activity of this fluid. Notably, the lighter O isotopic compositions occur in the upper and lower part of phosphate ore body in both of the Jinping and Xinpu section, inferring that the fluid reaction is strongest in the contact zone between the P-rich rocks and mica schists. In addition, the Xinpu P-rich rocks with a greater percentage of calcite veining and higher content of mica (H_2O-bearing minerals) are significantly lighter than that in the Jinping P-rich rocks, suggesting greater volumes of fluid interaction leads to the lower $\delta^{18}O$ values. Therefore, oxygen isotopes can be used as a very good proxy for tracing the involvement of metamorphic fluids.

5.2.2. The ^{66}Zn-depleted fluid recorded in metamorphosed phosphorites

The Zn isotopic fractionation is relatively common in low-temperature geochemical processes, such as adsorption, carbonate and phosphorite precipitation, and biological processes (John and Conway, 2014; Kunzmann et al., 2013; Vasileios et al., 2018). The Zn isotopic composition of marine sedimentary rocks is affected by continental weathering, submarine hydrothermal activity, marine productivity, and the redox state of water with detectable changes observed during major environmental biological events in geological history (Fan et al., 2018b; John et al., 2018; Kunzmann et al., 2013; Liu et al., 2017). Previous data indicate that there is a high degree of consistency in the variation of Zn isotopic compositions in different continental cap dolomites, indicating that the variation of Zn isotopic compositions in the early Ediacaran seawater is controlled by global factors, confirming that Zn isotope is a global paleoceanographic indicator (Kunzmann et al., 2013; Lv et al., 2018). Based on these observations, Zn isotopes in phosphorites deposited at the same time (i.e. Haizhou Group and Weng'an phosphorites) should yield similar values.

The Zn isotope compositions in the Weng'an phosphorites ($\delta^{66}Zn$ = ~0.8) have been well defined (Fan et al., 2018b). Compared to the high $\delta^{66}Zn$ values from the Weng'an phosphorites, the Xinpu and Jinping phosphorites have lighter Zn isotopic compositions (~0.36 in the Xinpu ore section, and ~ 0.58‰ in Jinping ore section). Interestingly, the metamorphosed phosphorites have higher Zn concentrations with lighter Zn isotopic compositions than those of the Weng'an phosphorite ore deposit, which suggests the light Zn isotopic compositions were trapped in the later subduction processes. The isotopic composition of zinc in Weng'an carbonate (~0.5‰) is close to that in seawater (Fan et al., 2018b).

The negative correlation between $\delta^{66}Zn$ and K, Rb, Ba, REY and Zn content (Fig. 9.A-E) confirms that this metamorphic fluid is exogenous. The clear correlation between $\delta^{66}Zn$ and $\delta^{18}O$ values (Fig. 9F) also suggests that the addition of the metamorphic fluids with lower $\delta^{18}O$ values also contain lighter Zn isotopic compositions. Modification of Zn values as evidenced by higher concentrations of Zn in Xinpu and Jinping sections with lighter Zn isotopic signatures, strongly support interaction of exogeneous metamorphic (subduction-zone) fluids with the Haizhou Group metasediments, particularly in contact with the overlying and underlying mica schists and basement rocks. Therefore, Zn isotopic

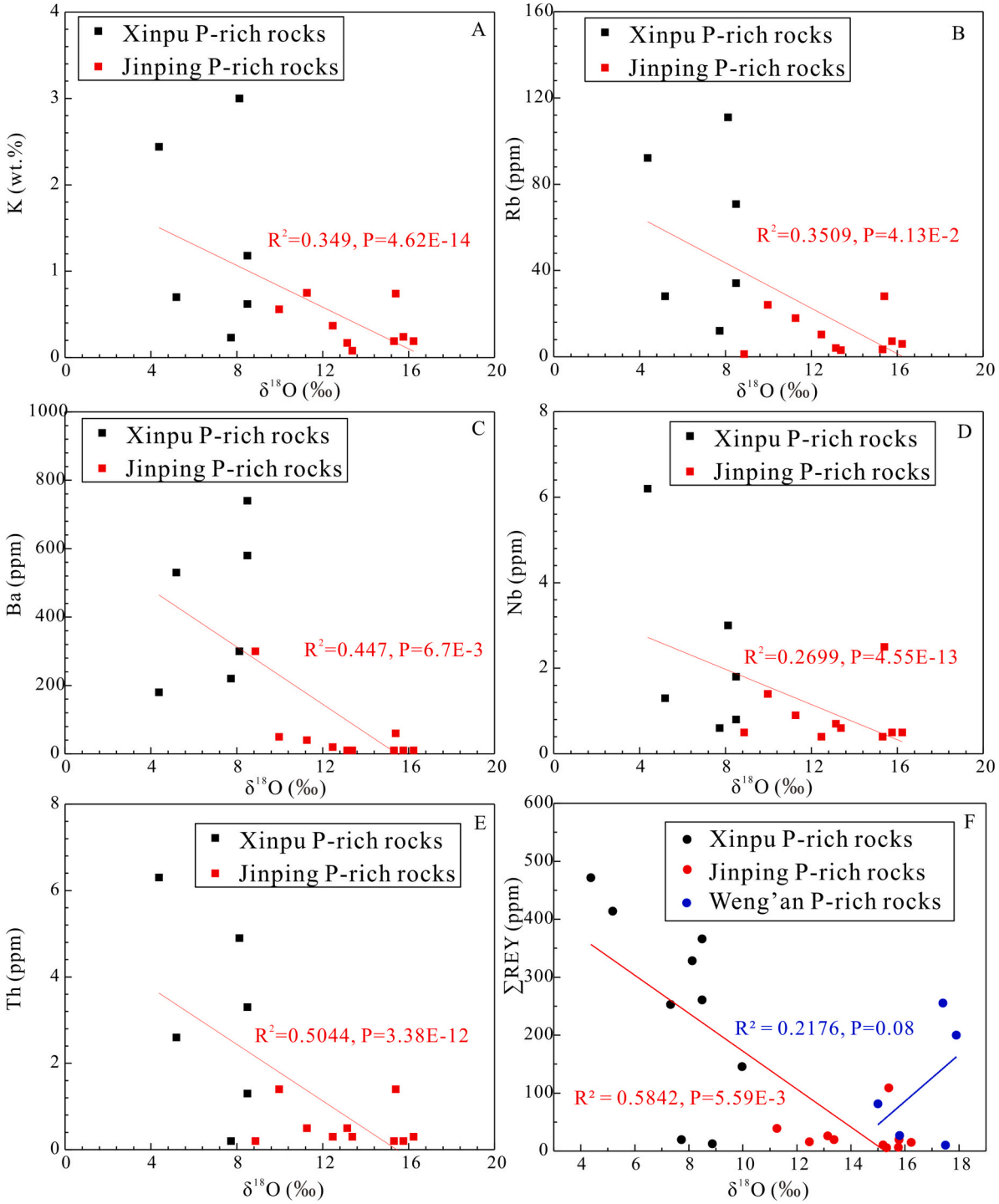

Fig. 8. A-E: The correlation diagrams of $\delta^{18}O$ vs. the content of K, Rb, Ba, Nb and Th of Haizhou P-rich rocks; F: The correlation diagrams of $\delta^{18}O$ vs. REY contents of Haizhou and Weng'an P-rich rocks (Yang et al., 2021).

composition can be also used as a good proxy to trace the metamorphic process and degree of phosphate rocks.

5.3. The remobilization mechanism of REY during metamorphism

There is a good negative correlation between the O isotope composition and REY content (Fig. 8F) of the Haizhou metamorphosed P-rich rocks, indicating that the participation of metamorphic fluids affects the secondary enrichment of REY, that is, the lighter the oxygen isotopic composition, the higher the REY content. Notably, this metamorphic fluid does not seem to be rich in high REY content, as high REY samples have not undergone significant changes. Therefore, during plate subduction, carbonaceous apatite reacts with metamorphic fluids, leading to REY activity. Later, REY re enriched during the recrystallization of carbonaceous apatite into fluorapatite, which may be the main mechanism of REY migration in Haizhou phosphate rocks. During this process, LREE is preferentially mobilised compared to HREE (Ishikawa et al., 2005; Zack and John, 2007), thus providing likely explanation for the greater enrichment of LREE and MREE in metamorphosed P-rich rocks.

Equilibrium between aqueous fluid and surrounding rock will only

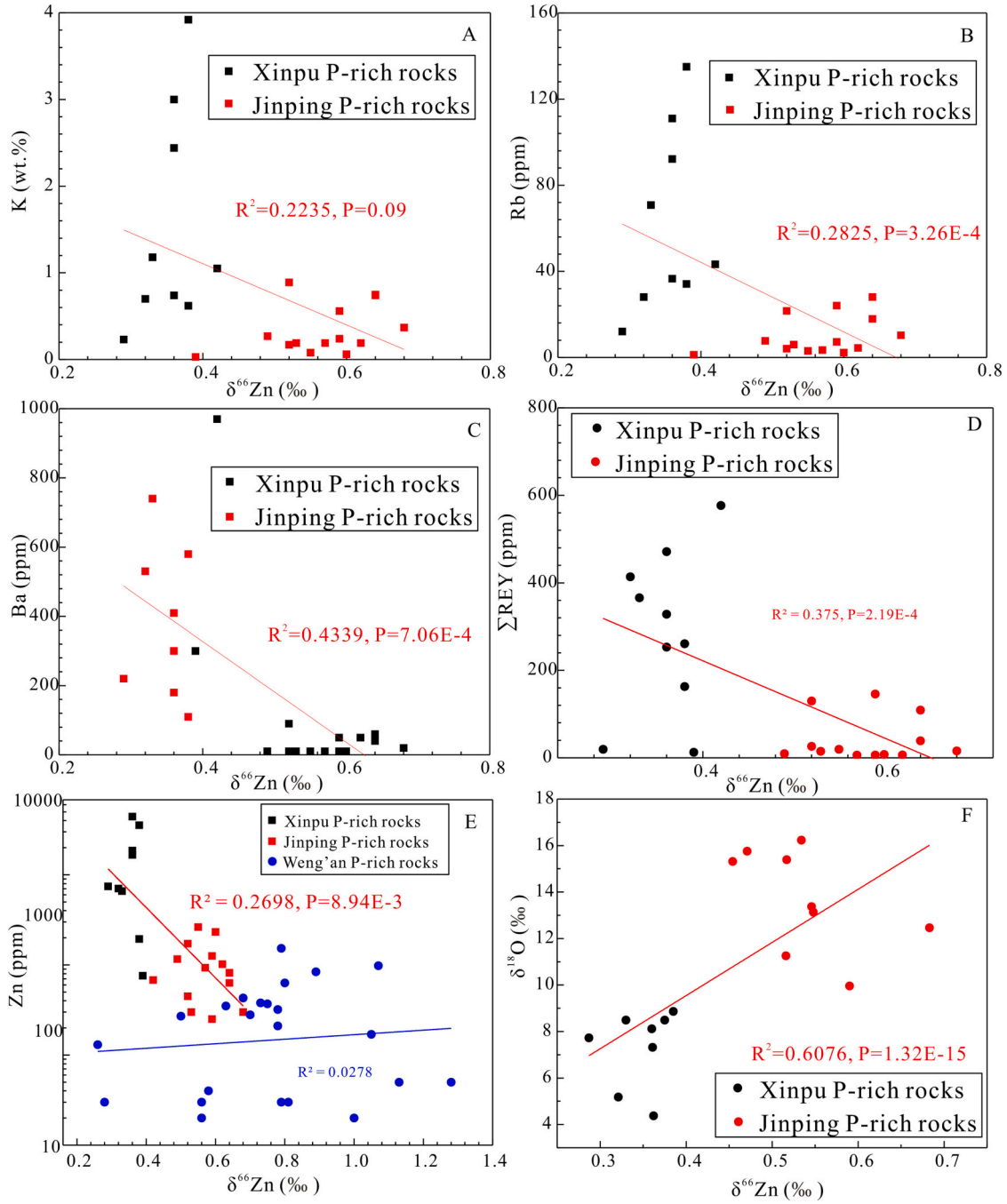

Fig. 9. A-D, F: The correlation diagrams of $\delta^{66}Zn$ vs. the content of K, Rb, Ba REY, and $\delta^{18}O$ of Haizhou P-rich rocks; E: The correlation diagrams of $\delta^{66}Zn$ vs. Zn contents of Haizhou and Weng'an P-rich rocks (Fan et al., 2018b).

be approached at sites of fluid production and mineral reaction (Zack and John, 2007). The highest REY contents, and lowest Zn and O isotope values were observed near the contacts of P-rich rocks with the mica-schists in the observed sections. The middle part of the sections yields overall lower values of REY and marginally higher O and Zn isotopes along with lower percentage of mica-rich rocks. During the process of converting clay minerals into mica, a decrease in solid volume, associated with dehydration reactions, increases porosity, and if sufficiently high volumes of fluid are reached, the elevated fluid pressure can open fractures to allow long-distance fluid transport(Jung et al., 2004; Zack and John, 2007). This suggests that fluid mediated REY enrichment and mobility is linked to zones with a high-production of metamorphic fluids during dehydration reactions involving mica-rich rocks. Furthermore, marbles at both sections display LREE-depleted values suggesting that some LREE in P-rich rocks (particularly low-REY apatite) may have been sourced by the recrystallisation of primary dolomites and limestones. Therefore, we propose that the metamorphosed phosphorites with high REY content still maintain the characteristics of the REY patterns of the original rocks in the upper and lower part of ore section, but the participation of $\delta^{18}O$ and $\delta^{66}Zn$ depleted fluids leads to the secondary enrichment of LREE and MREE (Fig. 10).

6. Conclusions

Both O and Zn isotopic compositions of metamorphosed phosphorites are lighter than those in unmetamorphosed phosphorites, which

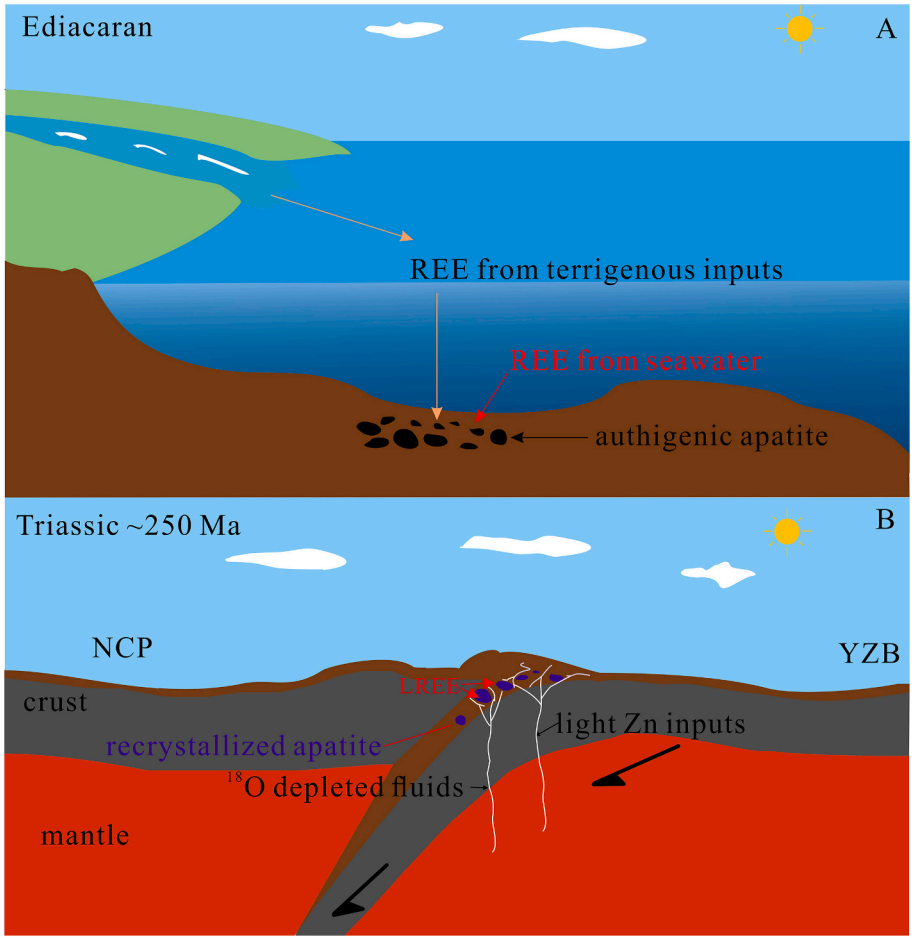

Fig. 10. Diagram of phosphorite metallogenesis in Ediacaran and Triassic.

could be controlled by varying degrees of water–rock reaction during metamorphism. These metamorphic fluids may be generated by the metamorphic dehydration of the metasedimentary rock pile during the plate subduction progress in the Triassic.

The good negative correlation between the O (and Zn) isotope compositions and REY contents in P-rich rocks, suggest that REY are re-enriched during the recrystallization process of apatite, and the stronger migration ability of LREE leads to significant LREE and MREE enrichment in Haizhou metamorphosed P-rich rocks compared to Weng'an unmetamorphosed phosphorites.

Declaration of Competing Interest

The authors declare that they have no known competing financial interests or personal relationships that could have appeared to influence the work reported in this paper.

Data availability

I have shared the data in at the Attach Files.

Acknowledgements

This work was supported by the National Natural Science Foundation of China (grant number 92062221, U1812402), Guizhou Provincial 2020 Science and Technology Subsides (GZ2020SIG), the Key R&D Program of Yunnan Province (202103AQ100003).

Appendix A. Supplementary data

Supplementary data to this article can be found online at https://doi.org/10.1016/j.chemgeo.2023.121781.

References

Algabri, M., She, Z.B., Jiao, L.X., et al., 2020. Apatite-glaucony association in the Ediacaran Doushantuo Formation, South China and implications for marine redox conditions. Precambrian Res. 347, 105842.
Bau, M., Moller, P., Dulski, P., 1997. Yttrium and lanthanides in eastern Mediterranean seawater and their fractionation during redox-cycling. Mar. Chem. 56 (1–2), 123–131.
Bindeman, I., 2008. 12. Oxygen Isotopes in Mantle and Crustal Magmas as Revealed by Single Crystal Analysis, pp. 445–478.
Blake, R.E., Chang, S.J., Lepland, A., 2010. Phosphate oxygen isotopic evidence for a temperate and biologically active Archaean Ocean. Nature. 464 (7291), 1029–1032.
Breeding, C.M., Ague, J.J., Brocker, M., 2004. Fluid-metasedimentary rock interactions in subduction-zone melange: Implications for the chemical composition of arc magmas. Geology 32 (12), 1041–1044.
Cawood, P.A., Zhao, G.C., Yao, J.L., et al., 2018. Reconstructing South China in Phanerozoic and Precambrian supercontinents. Earth Sci. Rev. 186, 173–194.
Chen, D.F., Dong, W.Q., Qi, L., et al., 2003. Possible REE constraints on the depositional and diagenetic environment of Doushantuo Formation phosphorites containing the earliest metazoan fauna. Chem. Geol. 201 (1), 103–118.
Chen, Y.X., Zheng, Y.F., Chen, R.X., et al., 2011. Metamorphic growth and recrystallization of zircons in extremely 18O-depleted rocks during eclogite-facies metamorphism: Evidence from U–Pb ages, trace elements, and O–Hf isotopes. Geochim. Cosmochim. Acta 75 (17), 4877–4898.
Chew, D.M., Babechuk, M.G., Cogne, N., et al., 2016. (LA,Q)-ICPMS trace-element analyses of Durango and McClure Mountain apatite and implications for making natural LA-ICPMS mineral standards. Chem. Geol. 435, 35–48.
Colman, A., 2002. The Oxygen Isotope Composition of Dissolved Inorganic Phosphate and the Marine Phosphorus Cycle. Ph.D. Yale University, New Haven, U.S.
Cook, P.J., Shergold, J.H., 1984. Phosphorus, Phosphorites and Skeletal Evolution at the Precambrian Cambrian Boundary. Nature. 308 (5956), 231–236.

Coplen, T.B., Kendall, C., Hopple, J., 1983. Comparison of stable isotope reference samples. Nature. 302 (5905), 236–238.
Cui, H., Kaufman, A.J., Xiao, S., et al., 2015. Redox architecture of an Ediacaran Ocean margin: Integrated chemostratigraphic (δ13C–δ34S–87Sr/86Sr–Ce/Ce*) correlation of the Doushantuo Formation, South China. Chem. Geol. 405, 48–62.
Cui, H., Xiao, S.H., Zhou, C.M., et al., 2016. Phosphogenesis associated with the Shuram Excursion: Petrographic and geochemical observations from the Ediacaran Doushantuo Formation of South China. Sediment. Geol. 341, 134–146.
Elderfield, H., Sholkovitz, E.R., 1987. Rare-Earth elements in the Pore Waters of reducing Nearshore Sediments. Earth Planet. Sci. Lett. 82 (3–4), 280–288.
Emsbo, P., McLaughlin, P.I., Breit, G.N., et al., 2015. Rare earth elements in sedimentary phosphate deposits: solution to the global REE crisis? Gondw. Res. 27 (2), 776–785.
Fan, H.F., Wen, H.J., Han, T., et al., 2018a. Oceanic redox condition during the late Ediacaran (551-541 Ma), South China. Geochim. Cosmochim. Acta 238, 343–356.
Fan, H.F., Wen, H.J., Xiao, C.Y., et al., 2018b. Zinc Geochemical Cycling in a Phosphorus-Rich Ocean during the early Ediacaran. J. Geophys. Res. Oceans 123 (8), 5248–5260.
Firsching, H.F., 1961. Precipitation of Silver Phosphate from Homogenous solution. Anal. Chem. 33 (7), 873–874.
Graham, S.-Z., Lawrence, O., 2011. The case for a Neoproterozoic Oxygenation Event: Geochemical evidence and biological consequences. GSA Today 21 (3), 4–11.
Hacker, B.R., Peacock, S.M., Abers, G.A., Holloway, S.D., 2003. Subduction factory 2. Are intermediate-depth earthquakes in subducting slabs linked to metamorphic dehydration reactions? J. Geophys. Res. Solid Earth. 108 (B1).
Ishikawa, T., Fujisawa, S., Nagaishi, K., Masuda, T., 2005. Trace element characteristics of the fluid liberated from amphibolite-facies slab: Inference from the metamorphic sole beneath the Oman ophiolite and implication for boninite genesis. Earth Planet. Sci. Lett. 240 (2), 355–377.
John, S.G., Conway, T.M., 2014. A role for scavenging in the marine biogeochemical cycling of zinc and zinc isotopes. Earth Planet. Sci. Lett. 394, 159–167.
John, S.G., Helgoe, J., Townsend, E., 2018. Biogeochemical cycling of Zn and Cd and their stable isotopes in the Eastern Tropical South Pacific. Mar. Chem. 201, 256–262.
Joosu, L., Lepland, A., Kirsimae, K., et al., 2015. The REE-composition and petrography of apatite in 2 Ga Zaonega Formation, Russia: the environmental setting for phosphogenesis. Chem. Geol. 395, 88–107.
Jung, H., Green Ii, H.W., Dobrzhinetskaya, L.F., 2004. Intermediate-depth earthquake faulting by dehydration embrittlement with negative volume change. Nature. 428 (6982), 545–549.
Kim, I., Kim, G., 2014. Submarine groundwater discharge as a main source of rare earth elements in coastal waters. Mar. Chem. 160, 11–17.
Kunzmann, M., Halverson, G.P., Sossi, P.A., et al., 2013. Zn isotope evidence for immediate resumption of primary productivity after snowball Earth. Geology. 41 (1), 27–30.
Li, S.Z., Kusky, T.M., Zhao, G.C., et al., 2011. Thermochronological constraints on two-stage extrusion of HP/UHP terranes in the Dabie-Sulu orogen, east-Central China. Tectonophysics. 504 (1–4), 25–42.
Liang, Q., Jing, H., Gregoire, D.C., 2000. Determination of trace elements in granites by inductively coupled plasma mass spectrometry. Talanta. 51 (3), 507–513.
Ling, H.F., Feng, H.Z., Pan, J.Y., et al., 2007. Carbon isotope variation through the neoproterozoic Doushantuo and Dengying formations, South China: Implications for chemostratigraphy and paleoenvironmental change. Palaeogeogr. Palaeoclimatol. Palaeoecol. 254 (1–2), 158–174.
Little, S.H., Vance, D., Walker-Brown, C., Landing, W.M., 2014. The oceanic mass balance of copper and zinc isotopes, investigated by analysis of their inputs, and outputs to ferromanganese oxide sediments. Geochim. Cosmochim. Acta 125 (15), 673–693.
Liu, F.L., Xu, Z.Q., Yang, J.S., et al., 2004. Geochemical characteristics and UHP metamorphism of granitic gneisses in the main drilling hole of Chinese Continental Scientific Drilling Project and its adjacent area. Acta Petrol. Sin. 20 (1), 9–26.
Liu, Y.S., Hu, Z.C., Gao, S., et al., 2008. In situ analysis of major and trace elements of anhydrous minerals by LA-ICP-MS without applying an internal standard. Chem. Geol. 257 (1–2), 34–43.
Liu, S.A., Wu, H.C., Shen, S.Z., et al., 2017. Zinc isotope evidence for intensive magmatism immediately before the end-Permian mass extinction. Geology. 45 (4), 343–346.
Liu, S.A., Qu, Y.R., Wang, Z.Z., et al., 2022. The fate of subducting carbon tracked by Mg and Zn isotopes: a review and new perspectives. Earth Sci. Rev. 228, 104010.
Liu, S.A., Li, D.D., Liu, W., et al., 2023. High-precision zinc isotope measurement of chemically different geostandards by multicollector inductively coupled plasma mass spectrometry. Rapid Commun. Mass Spectrom. 37 (17), e9606.
Lv, Y.W., Liu, S.A., Wu, H.C., et al., 2018. Zn-Sr isotope records of the Ediacaran Doushantuo Formation in South China: diagenesis assessment and implications. Geochim. Cosmochim. Acta 239, 330–345.
Manning, C., Ingebritsen, S., 1999. Permeability of the continental crust: Implications of geothermal data and metamorphic systems. Rev. Geophys. 37 (1), 127–150.
Martin, E.E., Scher, H.D., 2004. Preservation of seawater Sr and Nd isotopes in fossil fish teeth: bad news and good news. Earth Planet. Sci. Lett. 220 (1–2), 25–39.
Ohno, T., Komiya, T., Ueno, Y., et al., 2008. Determination of 88Sr/86Sr mass-dependent isotopic fractionation and radiogenic isotope variation of 87Sr/86Sr in the Neoproterozoic Doushantuo Formation. Gondw. Res. 14 (1–2), 126–133.
Prave, A.R., Meng, F.W., Lepland, A., et al., 2018. A refined late-Cryogenian - Ediacaran earth history of South China: Phosphorous-rich marbles of the Dabie and Sulu orogens. Precambrian Res. 305, 166–176.
Reynard, B., Lecuyer, C., Grandjean, P., 1999. Crystal-chemical controls on rare-earth element concentrations in fossil biogenic apatites and implications for paleoenvironmental reconstructions. Chem. Geol. 155 (3–4), 233–241.
Sang, L.K., 1991. The Petrochemistry of the lower Proterozoic Metamorphic Rocks from the Dabieshan Lianyungang Area, the Southeastern margin of the North China Platform. Mineral. Mag. 55 (379), 263–276.
Sato, H., Tahata, M., Sawaki, Y., et al., 2016. A high-resolution chemostratigraphy of post-Marinoan Cap Carbonate using drill core samples in the three Gorges area, South China. Geosci. Front. 7 (4), 663–671.
Schmidt, M.W., Poli, S., 1998. Experimentally based water budgets for dehydrating slabs and consequences for arc magma generation. Earth Planet. Sci. Lett. 163 (1), 361–379.
Shields, G., Stille, P., 2001. Diagenetic constraints on the use of cerium anomalies as palaeoseawater redox proxies: an isotopic and REE study of Cambrian phosphorites. Chem. Geol. 175 (1–2), 29–48.
Sossi, P.A., Nebel, O., O'Neill, H.S.C., Moynier, F., 2018. Zinc isotope composition of the Earth and its behaviour during planetary accretion. Chem. Geol. 477, 73–84.
Tahata, M., Ueno, Y., Ishikawa, T., et al., 2013. Carbon and oxygen isotope chemostratigraphies of the Yangtze platform, South China: Decoding temperature and environmental changes through the Ediacaran. Gondw. Res. 23 (1), 333–353.
Tang, S.H., Zhu, X.K., Cai, J.J., et al., 2006. Chromatographic Separation of Cu,Fe and Zn using AG MP-1 Anion Exchange Resin for Isotope Determination by MC-ICPMS. Rock and Mineral Analysis. 25 (1), 5–8 (in Chinese with English abstract).
Taylor, S.R., McLennan, S.M., 1985. The Continental Crust: Its Composition and Evolution. Blackwell Scientific Publication, Oxford, UK.
Valetich, M., Zivak, D., Spandler, C., et al., 2022. REE enrichment of phosphorites: an example of the Cambrian Georgina Basin of Australia. Chem. Geol. 588, 1–15.
Valley, J., 2019. Stable isotope geochemistry of metamorphic rocks, pp. 445–489.
Vance, D., Little, S.H., Archer, C., et al., 2016. The oceanic budgets of nickel and zinc isotopes: the importance of sulfidic environments as illustrated by the Black Sea. Philos. Trans. A. Math. Phys. Eng. Sci. 374 (2081), 20150294.
Vasileios, M., González, A., Martin, D., Jacques, S., 2018. Zinc isotope fractionation during the inorganic precipitation of calcite – Towards a new pH proxy. Geochim. Cosmochim. Acta 244, 99–112.
Wang, W.-H., Wong, T.-F., 2003. Effects of reaction kinetics and fluid drainage on the development of pore pressure excess in a dehydrating system. Tectonophysics. 370 (1), 227–239.
Wang, X.L., Zhou, J.C., Griffin, W.L., et al., 2014. Geochemical zonation across a Neoproterozoic orogenic belt: Isotopic evidence from granitoids and metasedimentary rocks of the Jiangnan orogen, China. Precambrian Res. 242, 154–171.
Wang, S.J., Wang, L., Brown, M., et al., 2017a. Fluid generation and evolution during exhumation of deeply subducted UHP continental crust: Petrogenesis of composite granite–quartz veins in the Sulu belt, China. Journal of Metamorphic Geology. 35 (6), 601–629.
Wang, Z.Z., Liu, S.A., Liu, J.G., et al., 2017b. Zinc isotope fractionation during mantle melting and constraints on the Zn isotope composition of Earth's upper mantle. Geochim. Cosmochim. Acta 198, 151–167.
Wen, H.J., Fan, H.F., Zhang, Y.X., et al., 2015. Reconstruction of early Cambrian Ocean chemistry from Mo isotopes. Geochim. Cosmochim. Acta 164, 1–16.
Xia, Q.X., Zheng, Y.F., Hu, Z.C., 2010. Trace elements in zircon and coexisting minerals from low-T/UHP metagranite in the Dabie orogen: Implications for action of supercritical fluid during continental subduction-zone metamorphism. Lithos. 114 (3), 385–412.
Xiong, X.X., Yao, C.M., 1996. Geological features and metallogenic model of Haizhou type phosphorite deposit. Mineral Deposits 15 (2), 171–181 (in Chinese with English abstract).
Xu, Z.Q., Zhang, Z.M., Liu, F.L., et al., 2003. Exhumation Structure and Mechanism of the Sulu Ultrahigh-pressure Metamorphic Belt, Central China. Acta Geol. Sin. 77 (04) (433-450+593-594 in Chinese with English abstract).
Yan, B., Zhu, X.K., He, X.X., Tang, S.H., 2019. Zn isotopic evolution in early Ediacaran Ocean: a global signature. Precambrian Res. 320, 472–483.
Yang, H.Y., Xiao, J.F., Xia, Y., et al., 2021. Phosphorite generative processes around the Precambrian-Cambrian boundary in South China: an integrated study of Mo and phosphate O isotopic compositions. Geosci. Front. 12 (5), 101187.
Yao, C.M., Xiong, X.X., 1994. Depositional conditions of Haizhou-type phosphate deposits. Geology of Chemical Minerals. 16 (04), 239–246 (in Chinese with English abstract).
Yu, L.M., Liu, M.X., Dan, Y., et al., 2023. The origin of Ediacaran phosphogenesis event: New insights from Doushantuo Formation in the Danzhai phosphorite deposit, South China. Ore Geol. Rev. 152, 105230.
Zack, T., John, T., 2007. An evaluation of reactive fluid flow and trace element mobility in subducting slabs. Chem. Geol. 239 (3), 199–216.
Zhang, H., Fan, H., Wen, H., et al., 2022. Controls of REY enrichment in the early Cambrian phosphorites. Geochim. Cosmochim. Acta 324, 117–139.
Zhao, G., Cawood, P.A., 2012. Precambrian geology of China. Precambrian Res. 222-223, 13–54.
Zheng, Y.F., Gong, B., Zhao, Z.F., et al., 2008a. Zircon U-Pb age and o isotope evidence for neoproterozoic low-18O magmatism during supercontinental rifting in South China: Implications for the snowball earth event. Am. J. Sci. 308 (4), 484–516.
Zheng, Y.F., Wu, R.X., Wu, Y.B., et al., 2008b. Rift melting of juvenile arc-derived crust: Geochemical evidence from Neoproterozoic volcanic and granitic rocks in the Jiangnan Orogen, South China. Precambrian Res. 163 (3), 351–383.

Zhou, J.B., Wilde, S.A., Liu, F.L., Han, J., 2012. Zircon U-Pb and Lu-Hf isotope study of the Neoproterozoic Haizhou Group in the Sulu orogen: Provenance and tectonic implications. Lithos. 136, 261–281.
Zhu, B., Jiang, S.Y., 2017. A LA-ICP-MS analysis of rare earth elements on phosphatic grains of the Ediacaran Doushantuo phosphorite at Weng'an, South China: implication for depositional conditions and diagenetic processes. Geol. Mag. 154 (6), 1381–1397.
Zong, K.Q., Liu, Y.S., Hu, Z.C., et al., 2010. Melting-induced fluid flow during exhumation of gneisses of the Sulu ultrahigh-pressure terrane. Lithos. 120 (3–4), 490–510.